Ceramics International xxx (xxxx) xxx

Contents lists available at ScienceDirect

Ceramics International

journal homepage: www.elsevier.com/locate/ceramint

Significantly enhanced sinterability and temperature stability of $Li_3Mg_4NbO_8$-based microwave dielectric ceramics with LiF and $Ba_3(VO_4)_2$ addition

Guoguang Yao *, Jingjing Tan, Jiaxin Yan, Meiqi Liu, Cuijin Pei, Yanmin Jia **

School of Science, Xi'an University of Posts and Telecommunications, Xi'an, 710121, China

ARTICLE INFO

Keywords:
Ceramic matrix composites
Microwave dielectric properties
LTCC

ABSTRACT

$Li_3Mg_4NbO_8$-basic composite ceramics were elaborated via the solid-state reaction process, in which LiF and $Ba_3(VO_4)_2$ were utilized as a sintering aid and reinforcement phase, respectively. The sinterability, phase assemblage, microstructures, and microwave dielectric performances of $Li_3Mg_4NbO_8$–LiF–$Ba_3(VO_4)_2$ composite ceramics were thoroughly researched. The co-addition of LiF–$Ba_3(VO_4)_2$ can simultaneously lower the sintering temperature and improve the thermal stability of $Li_3Mg_4NbO_8$-basic ceramics. Solid state activated sintering is responsible for the low-temperature densification of the present ceramics. The coexistence of rock-salt structural $Li_3Mg_4NbO_8$/$Li_4Mg_4NbO_8F$ and hexagonal structural $Ba_3(VO_4)_2$ phases was demonstrated by the combinational XRD and SEM-EDS analysis results. The 0.65($Li_3Mg_4NbO_8$–LiF)-0.35$Ba_3(VO_4)_2$ ceramics fired at 825 °C/5 h exhibited promising microwave dielectric performances: $\tau_f = 0.5$ ppm/°C along with $\varepsilon_r = 13.8$ and Qxf = 68500 GHz. The good compatibility of the developed ceramics with Ag demonstrates it potential for use in LTCC technology.

1. Introduction

As the prevalence of 5th generation (5G) wireless communication systems and Internet of Things, microwave dielectric ceramics have drawn special attentions because they are extensively applied as microwave passive devices including substrates of filters and antennas in wireless communication devices [1,2]. Besides, low-temperature co-fired ceramic (LTCC) technology is beneficial for realization the miniaturization and integration of future microwave devices [3–5]. To meet the requirements of 5G and LTCC technologies, dielectric ceramics should have two essential characteristics: (1) good dielectric performances including low permittivity (ε_r), low dielectric loss or high quality factor (Qxf), and small or zero temperature coefficient of resonant frequency (τ_f); (2) low firing temperature (≤960 °C) and excellent compatibility with Ag electrodes [6,7]. At present, numerous researches have been conducted to exploit new microwave dielectric ceramic systems, ameliorate the dielectric properties of specific ceramics via ion substitution or the formation of new composite materials, and reduce the firing temperature for specific ceramics by doping sintering aids [8–11].

Recently, rock-salt structural Li_2O–MgO–Nb_2O_5 system ceramics have attracted considerable attentions in commercial and scientific research owing to their fascinating dielectric and luminescence characteristics [12–16]. Our previous work showed that a new compound within the Li_2O–MgO–Nb_2O_5 system, namely, $Li_3Mg_4NbO_8$, was fabricated, it exhibited excellent dielectric performances at 9.6 GHz (ε_r = 13.8, Q × f = 103 400 GHz) [17]. However, the relative large negative τ_f value (−36 ppm/°C) and high sintering temperature (1150 °C) of $Li_3Mg_4NbO_8$ ceramics inhibited its use in LTCC applications. Previous researches demonstrate that LiF is a valid sintering aid for lowering the densification temperature of dielectric ceramics, particularly in Li-containing rock-salt structural ceramics [18–20]. For the abnormal low ε_r but positive τ_f values, the $Ba_3(VO_4)_2$ is often utilized as τ_f compensator in diphase ceramics such as $Ba_3(VO_4)_2$–$Ca_5Mg_4(VO_4)_6$, $Li_3Mg_2SbO_6$–$Ba_3(VO_4)_2$, etc [21,22].

In this paper, the LiF as sintering aid and $Ba_3(VO_4)_2$ as τ_f compensator were introduced to $Li_3Mg_4NbO_8$ ceramics, with the aim to concurrently obtain low sintering temperature and excellent dielectric performances of $Li_3Mg_4NbO_8$-basic ceramics. Therefore, we designed and prepared the 0.65($Li_3Mg_4NbO_8$–LiF)–0.35$Ba_3(VO_4)_2$ ceramics based

* Corresponding author.
** Corresponding author.
E-mail addresses: physicas@163.com (G. Yao), 469675491@qq.com (Y. Jia).

https://doi.org/10.1016/j.ceramint.2021.06.162
Received 26 April 2021; Received in revised form 14 June 2021; Accepted 19 June 2021
Available online 20 June 2021

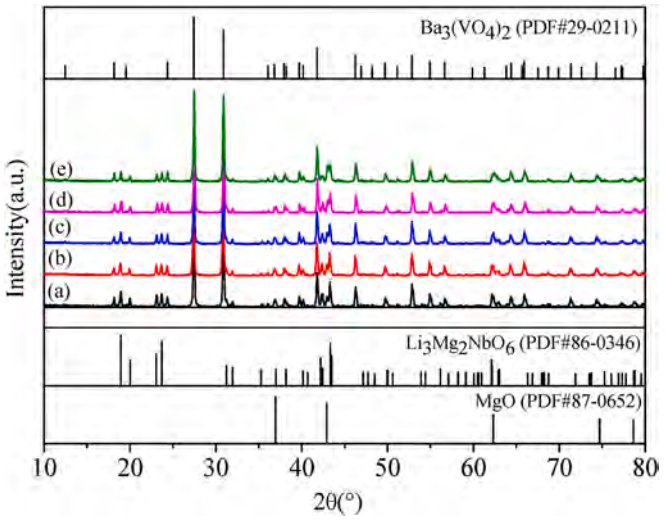

Fig. 1. XRD patterns of LMN-LiF-BV ceramics sintered at 750 °C–850 °C: (a) 750 °C, (b) 775 °C, (c) 800 °C, (d) 825 °C, (e) 850 °C.

on the mixing rule of τ_f and via a routine solid state reaction process [23]. Furthermore, we thoroughly investigated the impacts of $Ba_3(VO_4)_2$ and LiF addition on the phase purity, sinterability, microstructures, microwave dielectric characterization, and compatibility with silver electrode of $0.65(Li_3Mg_4NbO_8–LiF)–0.35Ba_3(VO_4)_2$ sintered bodies.

2. Experimental procedure

The $0.65(Li_3Mg_4NbO_8–LiF)$-$0.35Ba_3(VO_4)_2$ (abbreviated as LMN-LiF-BV) samples were elaborated via a classical solid-state process. The starting powders of MgO, Li_2CO_3, Nb_2O_5, $BaCO_3$, V_2O_5 **(all purity>99.0 %, Guo-Yao Co. Ltd., Shanghai, China)** were individually weighed according to stoichiometric $Li_3Mg_4NbO_8$ and $Ba_3(VO_4)_2$, then were separately mixed together for 8 h via planetary milling using zirconia and alcohol as media and solvent. The resultant milled powders of $Li_3Mg_4NbO_8$ and $Ba_3(VO_4)_2$ were presintered at 1000 °C/4 h and 650 °C/20 h, respectively. Then the LMN-LiF-BV mixture powders were remilled. The obtained powders were granulated using a 6 wt% PVA solution, and pelletized into green discs (Φ10 × 5 mm). These discs were sintered at 750 °C-850 °C for 5 h in air.

The phase constitutions of the LMN-LiF-BV ceramics were examined

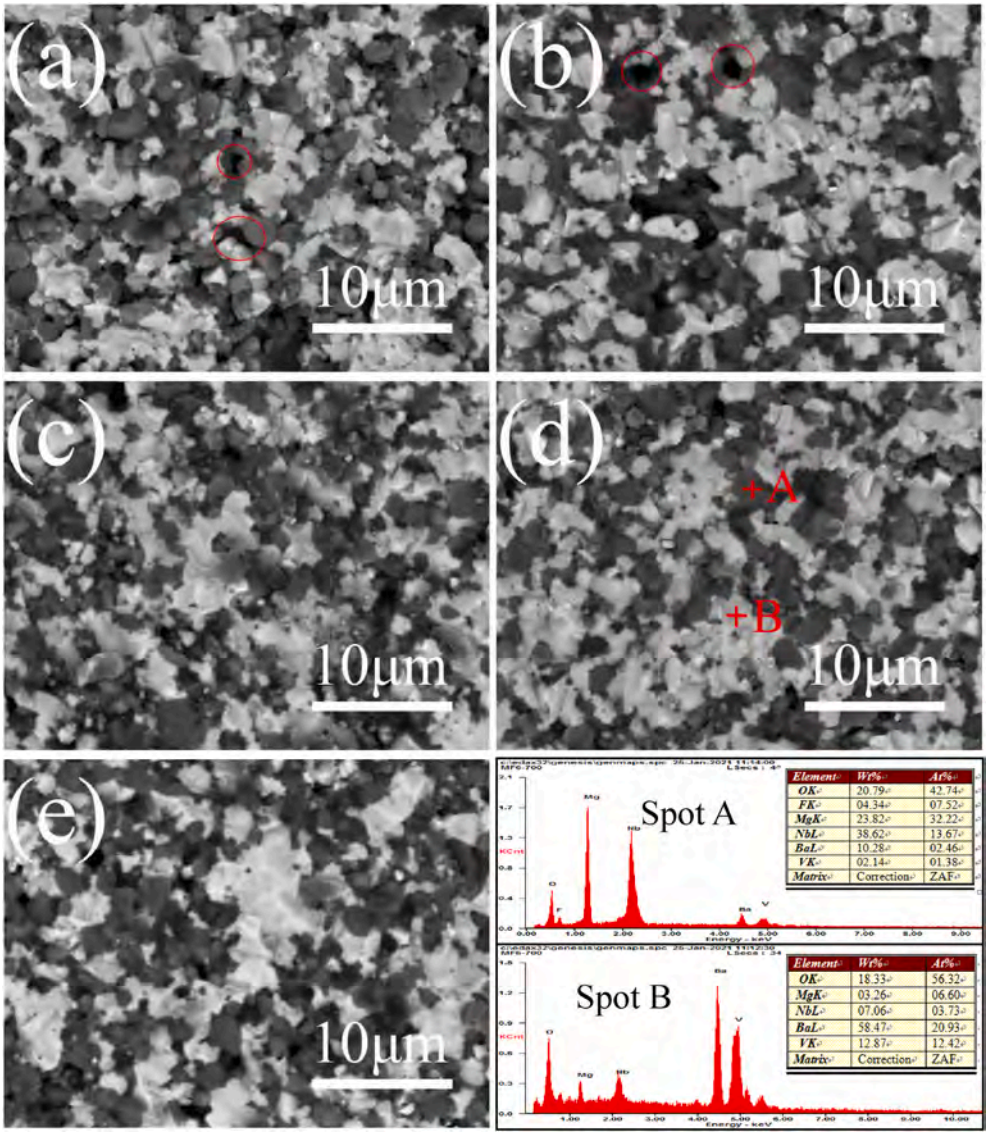

Fig. 2. The typical cross-section SEM images of LMN-LiF-BV ceramics sintered at different temperature: (a) 750 °C, (b) 775 °C, (c) 800 °C, (d) 825 °C, (e) 850 °C, and (f) EDS analysis of Fig. 2(d) points A and B.

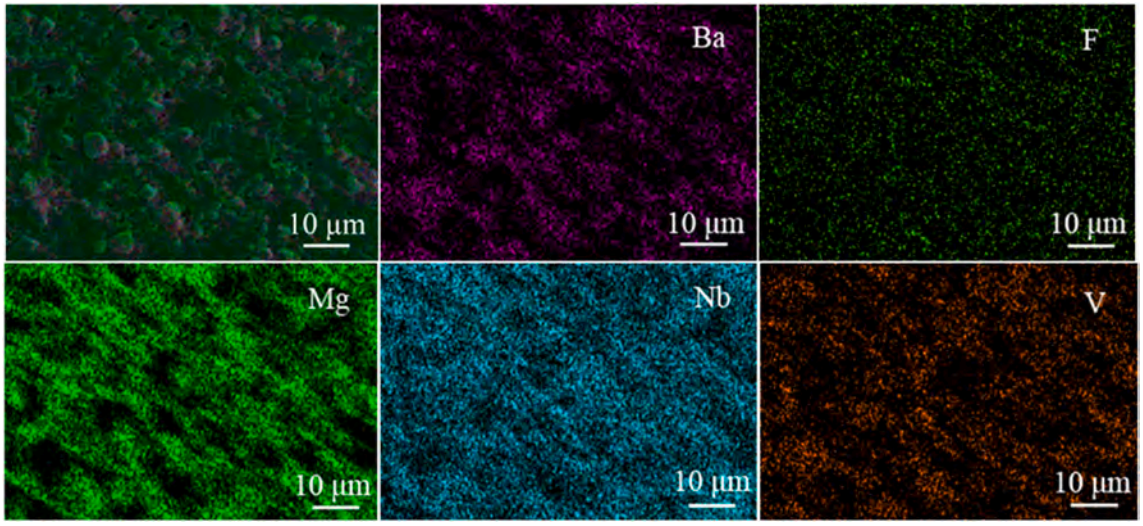

Fig. 3. Element mapping of Ba,V, Mg, Nb, F of LMN-LiF-BV ceramics sintered at 825 °C.

via X-ray powder diffraction (XRD, SmartLab, Japan). The fracture morphologies, and the main chemical composition of specimens were measured using a scanning electron microscope, (SEM, XL-40FEG, Philips) coupled with an energy-dispersive spectrometer (EDS). The apparent densities of sintered bodies were tested using Archimedes' principle. The ε_r and Qxf values of the LMN-LiF-BV ceramics were evaluated using a precision vector network analyzer (N5230A, Agilent, USA) under 9–10 GHz via the resonant cavity method. At 20 °C and 80 °C, the resonance frequency was tested to estimate the τ_f value using the following formula (1):

$$\tau_f = \frac{(f_{80} - f_{20}) \times 10^6}{f_{20} \times (80 - 20)} \quad (1)$$

3. Results and discussion

Fig. 1 presents the XRD profiles of $0.65(Li_3Mg_4NbO_8–LiF)–0.35Ba_3(VO_4)_2$ (LMN-LiF-BV) ceramics sintered at **750 °C–850 °C.** No significant change was found in the XRD patterns in all sintered bodies. The main diffraction peaks can be attributed to the $Ba_3(VO_4)_2$ phase (PDF#25-0902), and other diffraction peaks coincide with the orthorhombic $Li_3Mg_2NbO_6$-like (PDF#25-0902) or cubic MgO-like (PDF#87-0652) rock salt structure phase. The coexistence of cubic and orthorhombic rock salt phases and the absence of an obvious LiF phase indicated that the Li^+ and F^- ions entered the lattice of ordered orthorhombic $Li_3Mg_4NbO_8$, thus forming disordered cubic $Li_4Mg_4NbO_8F$. Similar phenomena were reported in other rock salt structure systems [1,24]. In addition, no additional phases emerged for all sintered specimens, except for the $Ba_3(VO_4)_2$, $Li_3Mg_4NbO_8$ and $Li_4Mg_4NbO_8F$ phases, thereby indicating the good compatibility of the $Li_3Mg_4NbO_8–Ba_3(VO_4)_2$ end-member. The good coexistence of $Li_3Mg_4NbO_8–Ba_3(VO_4)_2$ composite ceramics can be ascribed to their different crystal structures, which is favor of compensating for the dielectric properties of $Li_3Mg_4NbO_8$-basic ceramics, especially for τ_f [21].

The morphological microstructures of LMN-LiF-BV composite ceramics sintered at different temperatures are presented in Fig. 2. When the specimens were heated at a temperature under 800 °C or above 850 °C, large intergranular pores (as indicated by red circles) or uneven grain-size distribution were observed. As shown in Fig. 2 (d), a relatively compact microstructure with few pores was achieved, which corresponds to the saturated bulk density and dielectric properties (Fig. 3). Meanwhile, all specimens exhibited similar grain sizes and two different-colored grains (bright and dark), which possibly denote distinct phase assemblages [25]. Thus, EDS spectra were performed on the 825 °C-sintered LMN-LiF-BV ceramics as a representative to assess the phase assemblage for the different-colored grains. As shown in the EDS spectra of Fig. 2(f), the dark grains (spot A) are rich in Mg, F and Nb but relatively poor in Ba, and V, whereas the bright grains (spot B) are rich in Ba and V but relatively poor in Mg, F and Nb. In combination with the XRD results and considering the fact that the Li element is too light to be detected, the dark and bright grains corresponded approximately to $Li_3Mg_4NbO_8/Li_4Mg_4NbO_8F$ and $Ba_3(VO_4)_2$, respectively. Furthermore, SEM mapping was used to exhibit the element distribution. As revealed by the element mapping in Fig. 3, Mg, Nb and F elements are mainly distributed in the dark grains, whereas Ba and V elements are mainly distributed in the bright grains, respectively. The element mapping results are consistent with the EDS spectra results.

Fig. 4 illustrates the variation of bulk density (ρ) and dielectric performances (ε_r, Q × f, τ_f) of LMN-LiF-BV ceramics with respect to sintering temperature. The ρ value rose gradually, and reached the saturated value at approximately 825 °C as increasing sintering temperature. The variations of ρ are consistent with the microstructure of SEM observation. The variation tendency of the ε_r values of the LMN-LiF-BV ceramics was the same as that of the ρ because a high ρ corresponds to a high ε_r [26]. As shown in Fig. 4(b), the Qxf value for LMN-LiF-BV ceramics rose initially, reached the saturated value at around 825 °C, and then declined with increasing temperature, although its ρ slightly increased. In general, the Qxf value of microwave ceramics

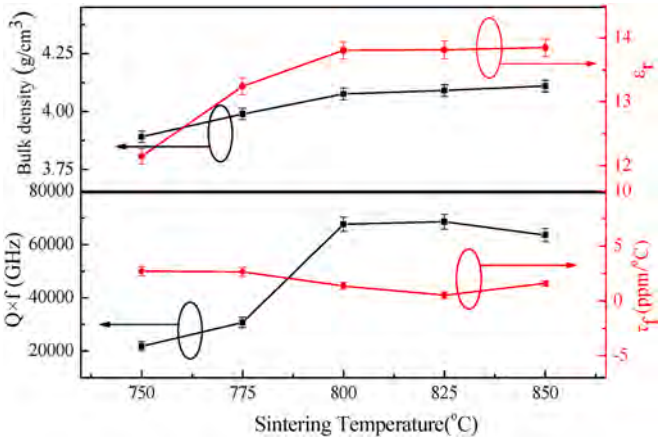

Fig. 4. Dependence of ρ, ε_r, Q × f and τ_f of LMN-LiF-BV ceramics on sintering temperature.

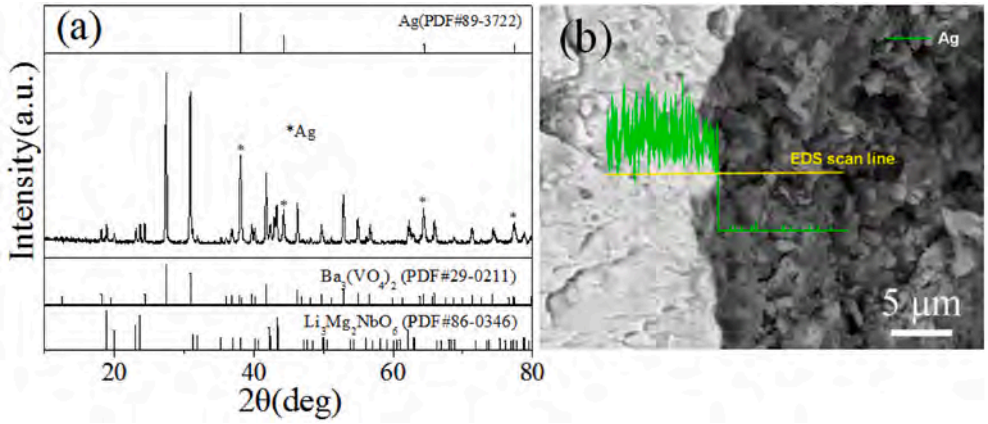

Fig. 5. The XRD pattern, interface morphology and EDS line scan of LMN-LiF-BV-20 wt% Ag sample sintered at 825 °C.

is primarily affected by extrinsic factors, such as impurity phases, bulk density, and defects [27–29]. In our case, the increment in the Qxf value can be attributed to the improvement of the density, whereas the decline of the Qxf value is possible because of the defect caused by exaggerated grain growth [30]. As illustrated in Fig. 4(b), the impaction of sintering temperature on the τ_f values of LMN-LiF-BV seemed to be small, and the τ_f value remained stable at approximately 1.0 ppm/°C because no remarkable changes were observed in constitutions (Fig. 1). In summary, the optimum dielectric properties were achieved for LMN-LiF-BV ceramics sintered at 825 °C. The densification temperature (825 °C) of the present ceramics is lower than the melting point (850 °C) of LiF [31]. Thus, we infer that the low temperature sintering mechanism of present ceramics is solid-state activated sintering [32]. Specifically, the incorporation of LiF into the $Li_3Mg_4NbO_8$ lattice decreased the chemical potential, thus reducing the firing temperature for the present samples [31–33].

To assess the suitability of LMN-LiF-BV ceramics in LTCC application, its chemical compatibility with Ag electrode was examined. Fig. 5 displays the XRD pattern along with the interface morphology and EDS line scan of LMN-LiF-BV with 20 wt% Ag addition sintered at 825 °C. No other additional phase besides LMN-BV composite ceramics and Ag phases could be obviously detected from the XRD pattern in Fig. 5(a). This indicated that no chemical reaction occurred between them during the sintering process. Furthermore, no delamination and element diffusion phenomena were observed at the interface between the LMN-LiF-BV ceramics and the Ag electrode, as shown in Fig. 5(b). These characters demonstrate that the LMN-LiF-BV ceramics could be well matched with the Ag electrode. Moreover, Table 1 summarizes the microwave dielectric properties and optimal firing temperature of some ceramics in the Li_2O–MgO–Nb_2O_5 system. As shown in Table 1, our $Li_3Mg_4NbO_8$-LiF-BV ceramics exhibit a lower sintering temperature or higher Qxf value compared with **other related ceramics.** Thus, the foreseeable potential of LMN-LiF-BV ceramics for LTCC applications should be expected.

Table 1
Comparison of the proposed dielectrics with some compounds in Li_2O–MgO–Nb_2O_5 system.

Compounds	ε_r	Q × f (GHz)	τ_f (ppm/°C)	ST (°C)	Ref.
0.65($Li_3Mg_4NbO_8$–LiF) -0.35$Ba_3(VO_4)_2$	13.8	68500	0.5	825	[a]
Li_3MgNbO_5–$CaTiO_3$	18.4	86625	1.2	1260	[14]
0.7$Li_3(Mg_{0.92}Zn_{0.08})_2NbO_6$ -0.3$Ba_3(VO_4)_2$	16.3	50084	1.5	950	[34]
$Li_3Mg_2NbO_6$-0.1TiO_2-LBBS	16.0	42648	-1.0	900	[35]
$Li_3Mg_2(Nb_{0.94}W_{0.06})O_{6.03}$	15.8	124187	-18.3	1175	[36]
$Li_3Mg_2(Nb_{0.94}Nb_{0.06})O_6$	15.8	95487	-24.3	1150	[37]

[a] This work.

4. Conclusions

New temperature-stable LMN-LiF-BV diphase ceramics **were prepared** via the solid-state reaction process. The impacts of LiF–$Ba_3(VO_4)_2$ introduction on the phase assemblage, firing behavior, microstructures, and microwave dielectric characteristics of $Li_3Mg_4NbO_8$-basic ceramics were systematically researched. The remarkably low sintering temperature and favorable thermal stability of $Li_3Mg_4NbO_8$-basic ceramics can be attributed to the introduction of LiF and $Ba_3(VO_4)_2$, respectively. XRD and SEM-EDS analyses confirmed that the rock salt structural ($Li_3Mg_4NbO_8$, $Li_4Mg_4NbO_8F$) and hexagonal structural $Ba_3(VO_4)_2$ phases can stably coexist. Typically, the optimal microwave dielectric characteristics were achieved for LMN-LiF-BV ceramics sintered at 825 °C, where ε_r = 13.8, Qxf = 68500 GHz **(at 9.4 GHz)**, and τ_f = 0.5 ppm/°C. Besides, the good compatibility of the present ceramics with Ag further makes it a potential alternative material for LTCC technology.

Declaration of competing interest

The authors declare that they have no known competing financial interests or personal relationships that could have appeared to influence the work reported in this paper.

Acknowledgements

The authors acknowledge supports from National Natural Science Foundation of China (Grant No 52002317), Shaanxi Province Natural Science Foundation, China (Grant No. 2021JM-458) and Xi'an of Science and technology Bureau (GXYD17.19).

References

[1] X. Chu, J. Jiang, J.Z. Wang, Y.C. Wu, L. Gan, T.J. Zhang, A new high-Q×f Li_4NbO_4F microwave dielectric ceramic for LTCC applications, Ceram. Int. 47 (2021) 4344–4351.
[2] L.Y. Ao, Y. Tang, J. Lia, W.S. Fang, L. Duan, C.X. Su, Y.H. Sun, L.J. Liu, L. Fang, Structure characterization and microwave dielectric properties of $LiGa_5O_8$ ceramic with low-ε_r and low loss, J. Eur. Ceram. Soc. 40 (2020) 5498–5503.
[3] D.W. Wang, L.H. Li, J. Jiang, Z.L. Lu, G. Wang, K.X. Song, D. Zhou, I.M. Reaney, Cold sintering of microwave dielectric ceramics and devices, J. Mater. Res. 36 (2021) 333–349.
[4] Y.W. Chen, E.Z. Li, S.X. Duan, S.R. Zhang, Low temperature sintering kinetics and microwave dielectric properties of $BaTi_5O_{11}$ ceramic, ACS Sustain. Chem. Eng. 5 (2017) 10606–10613.
[5] H.I. Hsiang, C.C. Chen, S.Y. Yang, Microwave dielectric properties of $Ca_{0.7}Nd_{0.2}TiO_3$ ceramic-filled CaO-B_2O_3-SiO_2 glass for LTCC applications, J. Adv. Ceram. 8 (2019) 345–351.

[6] H. Ohsato, J. Varghese, A. Kan, J.S. Kim, I. Kagomiya, H. Ogawa, M.T. Sebastian, H. Jantunen, Volume crystallization and microwave dielectric properties of indialite/cordierite glass by TiO_2 addition, Ceram. Int. 47 (2021) 2735–2742.
[7] H.Y. Yang, S.R. Zhang, H.C. Yang, E.Z. Li, Usage of P-V-L bond theory in studying the structural/property regulation of microwave dielectric ceramics: a review, Inorg. Chem. Front. 7 (2020) 4711–4753.
[8] A. Goulas, G. Chi-Tangyie, D.W. Wang, S.Y. Zhang, A. Ketharam, Microstructure and microwave dielectric properties of 3D printed low loss $Bi_2Mo_2O_9$ ceramics for LTCC applications, Appl. Mater. Today. 21 (2020) 100862.
[9] Z.B. Feng, B.J. Tao, W.F. Wang, H.Y. Liu, H.T. Wu, Z.L. Zhang, Sintering behavior and microwave dielectric properties of $Li_4Mg_3[Ti_{0.8}(Mg_{1/3}Ta_{2/3})_{0.2}]_2O_9$ ceramics with LiF additive for LTCC applications, J. Alloys Compd. 822 (2020) 153634.
[10] H.Y. Yang, S.R. Zhang, Y.W. Chen, H.C. Yang, Y. Yuan, E.Z. Li, Crystal chemistry, Raman spectra, and bond characteristics of Trirutile-Type $Co_{0.5}Ti_{0.5}TaO_4$ microwave dielectric ceramics, Inorg. Chem. 58 (2019) 968–976.
[11] H.H. Guo, M.S. Fu, D. Zhou, C. Du, P.J. Wang, Design of a high-efficiency and -gain antenna using novel low-loss, temperature-stable $Li_2Ti_{1-x}(Cu_{1/3}Nb_{2/3})_xO_3$ microwave dielectric ceramics, ACS Appl. Mater. Interfaces 13 (2021) 912–923.
[12] M. Castellanos, J.A. Gard, A.R. West, Crystal data for a new family of phases, $Li_3Mg_2XO_6$: X=Nb, Ta, Sb, J. Appl. Crystallogr. 15 (1982) 116–119.
[13] L.L. Yuan, J.J. Bian, Microwave dielectric properties of the lithium containing compounds with rock salt structure, Ferroelectrics 387 (2009) 123–129.
[14] J. Li, Z.W. Zhang, Y.F. Tian, L.Y. Ao, J.Q. Chen, et al., Crystal structure and microwave dielectric properties of a novel rock-salt type Li_3MgNbO_5 ceramic, J. Mater. Sci. 55 (2020) 15643–15652.
[15] X.C. Wang, X.P. Zhou, Y.X. Cao, Q. Wei, Z.Y. Zhao, Y.H. Wang, Insight into a novel rare-earth-free red-emitting phosphor $Li_3Mg_2NbO_6:Mn^{4+}$: structure and luminescence properties, J. Am. Ceram. Soc. 102 (2019) 6724–6731.
[16] X. Zhang, Z.X. Fang, H.Y. Yang, P. Zhao, X. Zhang, Y.P. Li, Lattice evolution, ordering transformation and microwave dielectric properties of rock-salt $Li_{3+x}Mg_{2-2x}Nb_{1-x}Ti_{2x}O_6$ solid-solution system: a newly developed pseudo ternary phase diagram, Acta Mater. 206 (2021) 116636.
[17] G.G. Yao, C.J. Pei, et al., Wide sintering temperature range Microwave dielectric ceramic with low loss and its preparation method, China Patent, 202010833809.8, 2020-08-19.
[18] R.Z. Zuo, J. Zhang, J. Song, Y.D. Xu, Liquid-phase sintering, microstructural evolution, and microwave dielectric properties of $Li_2Mg_3SnO_6$-LiF ceramics, J. Am. Ceram. Soc. 101 (2018) 569–576.
[19] G. Wang, D.N. Zhang, Y.M. Lai, X. Huang, Q.Q. Wang, C. Liu, H.W. Zhang, Ultralow loss and temperature stability of $Li_3Mg_2NbO_6$-xLiF ceramics with low sintering temperature, J. Alloys Compd. 782 (2018) 370–374.
[20] A. Kan, T. Moriyama, S. Takahashi, H. Ogawa, Low-temperature sintering and microwave dielectric properties of MgO ceramic with LiF Addition, J. Appl. Phys. 50 (2011) 1489–1496.
[21] G.G. Yao, C.J. Pei, H. Ma, J.G. Xu, P. Liu, H.W. Zhang, Low-temperature firing and microwave dielectric properties of (1-x)$Ca_5Mg_4(VO_4)_6$-x$Ba_3(VO_4)_2$ temperature stable ceramics, J. Alloys Compd. 709 (2017) 234–239.
[22] G.G. Yao, C.J. Pei, Y. Gong, Z.Y. Ren, P. Liu, Microwave dielectric properties of temperature stable (1-x)$Li_3Mg_2SbO_6$-x$Ba_3(VO_4)_2$ ceramics, J. Mater. Sci. Mater. Electron. 29 (2018) 9979–9983.
[23] R. Freer, F. Azough, Microstructural engineering of microwave dielectric ceramics, J. Eur. Ceram. Soc. 28 (2008) 1433–1441.
[24] Z.W. Zhang, Y. Tang, H.C. Xiang, A.H. Yang, Y. Wang, C.Z. Yin, Y.F. Tian, L. Fang, $Li_5Ti_2O_6F$: a new low-loss oxyfluoride microwave dielectric ceramic for LTCC applications, J. Mater. Sci. 55 (2020) 7485–7489.
[25] C.J. Pei, Y. Li, J.J. Tan, G.G. Yao, Y.M. Jia, Temperature stable (1-x)$NaCa_4V_5O_{17}$-xBaV_2O_6 microwave dielectric ceramics for ULTCC applications, Ceram. Int. 17 (2017) 27579–27583.
[26] S.J. Penn, N.M. Alford, A. Templeton, X. Wang, Effect of porosity and grain Size on the microwave dielectric properties of sintered Alumina, J. Am. Ceram. Soc. 80 (1997) 1885–1888.
[27] K. Du, J. Fan, Z.Y. Zou, X.Q. Song, W.Z. Lu, W. Lei, Crystal structure, phase compositions, and microwave dielectric properties of malayaite-type $Ca_{1-x}Sr_xSnSiO_5$ ceramics, J. Am. Ceram. Soc. 103 (2020) 6369–6377.
[28] Q. Zhang, H. Su, M.F. Zhong, Y.X. Li, X.L. Tang, Y.L. Jing, Bond characteristics and microwave dielectric properties on $Zn_{3-x}Cu_x(BO_3)_2$ ceramics with ultralow dielectric loss, Ceram. Int. 47 (2020) 4466–4474.
[29] H.C. Yang, S.R. Zhang, H.Y. Yang, Y. Yuan, E.Z. Li, Vibrational spectroscopic and crystal chemical analyses of double perovskite Y_2MgTiO_6 microwave dielectric ceramics, J. Am. Ceram. Soc. 103 (2020) 1121–1130.
[30] N.M. Alford, J. Breeze, X. Wang, S.J. Penn, S. Dalla, S.J. Webb, N. Ljepojevic, X. Aupi, Dielectric loss of oxide single crystals and polycrystalline analogues from 10 to 320 K, J. Eur. Ceram. Soc. 21 (2001) 2605–2611.
[31] K. Xiao, C.C. Li, Y. Tang, Y.F. Tian, C.Z. Yin, J.Q. Chen, J. Li, L. Duan, H.C. Xiang, L. Fang, (1-x)Li4WO5-xLiF: a novel oxyfluoride system and their microwave dielectric properties, J. Alloys Compd. 835 (2020) 155320.
[32] K. Shigeno, Y. Kuraoka, T. Asakawa, H. Fujimori, Sintering mechanism of low-temperature co-fired alumina featuring superior thermal conductivity, J. Am. Ceram. Soc. 104 (2020) 2017–2029.
[33] P. Zhang, M.M. Yang, M. Xiao, Z.T. Zheng, Sintering behavior and microwave dielectric properties of $Li_2Mg_3Ti(O_{1-x/2}F_x)_6$ ($0.06 \leq x \leq 0.15$) ceramics for LTCC application, Mater. Chem. Phys. 236 (2019) 121805.
[34] T.W. Zhang, R.Z. Zuo, C. Zhang, Preparation and microwave dielectric properties of $Li_3(Mg_{0.92}Zn_{0.08})_2NbO_6$-$Ba_3(VO_4)_2$ composite ceramics for LTCC applications, Mater. Res. Bull. 68 (2015) 109–114.
[35] G. Wang, H.W. Zhang, C. Liu, H. Su, J. Li, X. Huang, G.W. Gan, F. Xu, Low temperature sintering and microwave dielectric properties of novel temperature stable $Li_3Mg_2NbO_6$-0.1TiO_2 ceramics, Mater. Lett. 217 (2018) 48–51.
[36] P. Zhang, M.M. Hao, X.R. Mao, K.X. Sun, M. Xiao, Effects of W^{6+} substitution on crystal structure and microwave dielectric properties of $Li_3Mg_2NbO_6$ ceramics, Ceram. Int. 46 (2020) 21336–21342.
[37] P. Zhang, S.X. Wu, M. Xiao, Effect of Sb^{5+} ion substitution for Nb^{5+} on crystal structure and microwave dielectric properties for $Li_3Mg_2NbO_6$ ceramics, J. Alloys Compd. 766 (2018) 498–505.